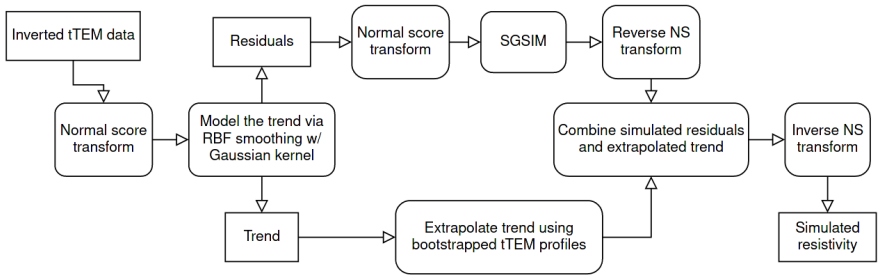

Figure S1. The full geostatistical workflow used to interpolate and extrapolate an inversion of the tTEM data onto a rectilinear grid. First, the resistivity model is transformed to a Gaussian distribution via rank transformation. Next, the trend is modeled using a radial basis function (RBF) with Gaussian kernel and values are decomposed into trend and residual components. Sequential Gaussian simulation (SGSIM) is then used to generate realizations of the stationary residuals. The trend is extrapolated using bootstrapped 1D profiles from within the domain (section 3.2.2), combined with the realizations of the residuals. Finally, the residuals and trend are added together and inverse transformed.

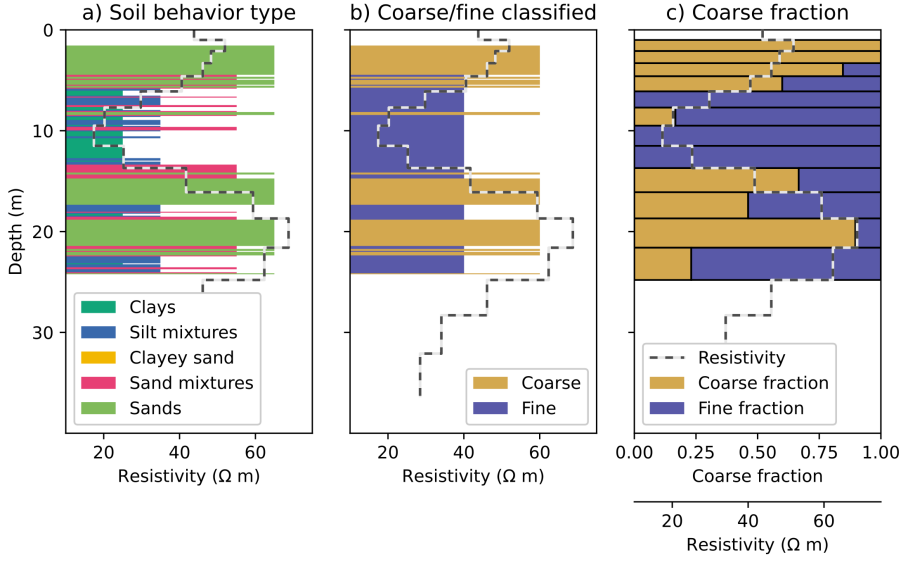

Figure S2. An example cone penetration test (CPT) log used to develop the resistivity-lithology model for transforming resistivity to coarse fraction. Normalized soil behavior types from each CPT depth interval (a) are classified as either fine- or coarse-grained (b). The classified logs are then upsampled to the resolution of the tTEM resistivity model (c) by calculating the percent of coarse-grained CPT observations within each tTEM pixel. Resistivity from the nearest inverted tTEM sounding is plotted in black and white over each log. The CPT logging interval was 10 cm.

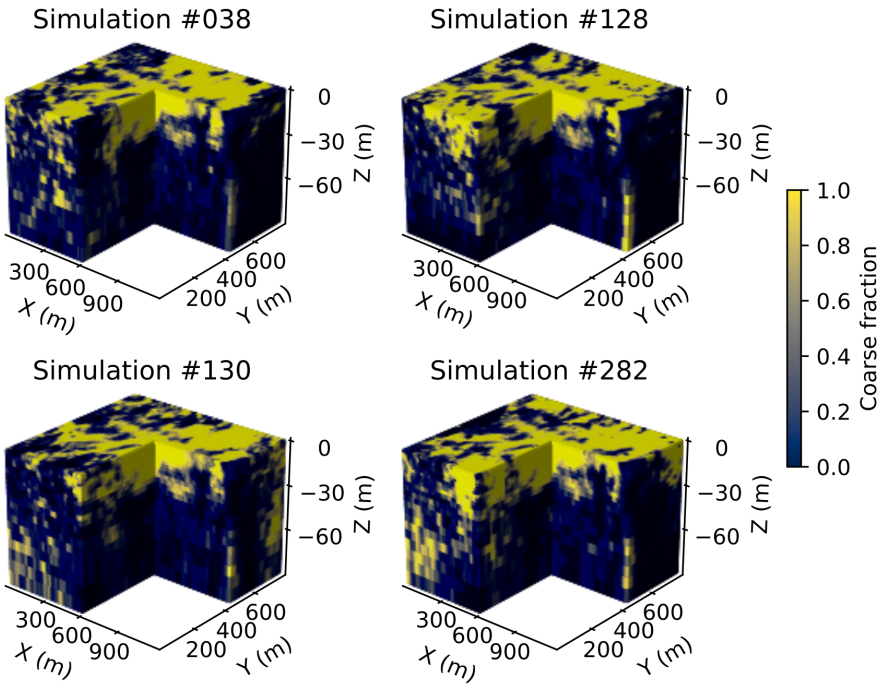

Figure S3. Four example coarse fraction realizations generated using the workflow described in the main text. Each realization extends from 0 to 90 m depth and is shown with 10x vertical exaggeration.

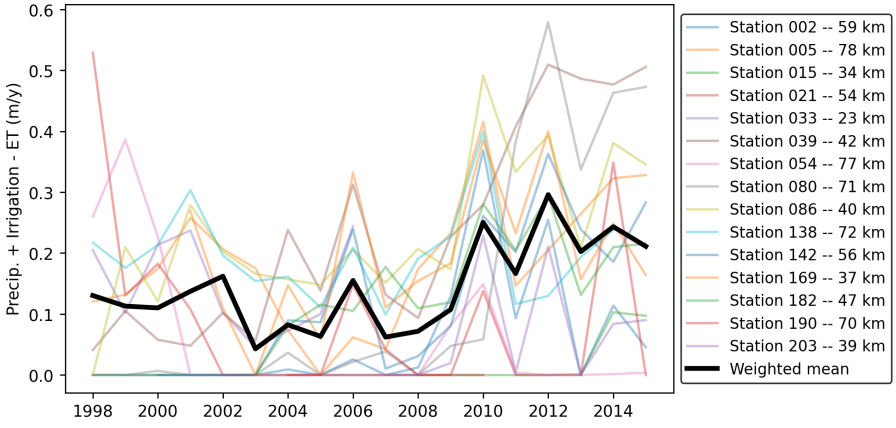

Figure S4. Annual net recharge rate from a hypothetical Central Valley almond orchard, using precipitation and reference evapotranspiration data from the 15 nearest CIMIS (California Irrigation Management Information System) stations to the field site. The black line is the weighted mean of individual rates calculated from each station, with stations weighted according to their proximity to the site. The legend includes each station number, as well as its distance from the field site in kilometers.

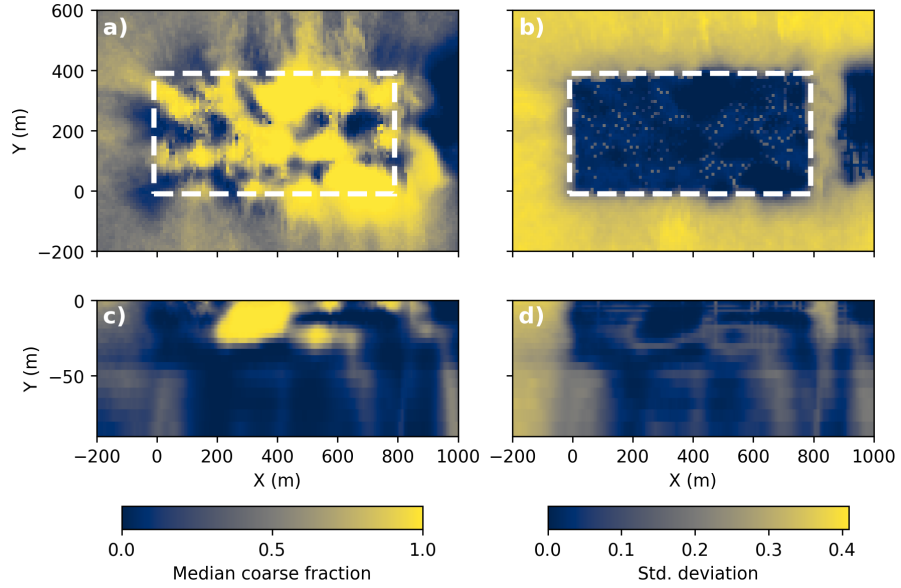

Figure S5. The median (a, c) and standard deviation (b, d) of coarse fraction across all 600 stochastic realizations. The top two subplots (a, b) show a top-down view of the surface layer of model cells, while the bottom two plots (c, d) show a vertical cross-section through the domain at x = 200 m. The white rectangle indicates the bounds of the almond orchard.

Table S1. Effect of domain size on errors in subsurface storage and outcomes of interest.

		Subsurface storage error		Errors in outcomes of interest		
Padding	# of cells	Spinup	Inundation	Infiltration	RZ res. time	Recharge pct.
200 m	240,000	-0.21%	-0.22%	0.00%	0.00%	10.4%
500 m	630,000	-0.14%	-0.15%	0.00%	0.00%	3.8%
700 m	990,000	-0.10%	-0.10%	0.00%	0.00%	3.2%
1000 m	1,680,000	N/A	N/A	N/A	N/A	N/A

Each value represents the percent difference between a given simulation and the simulation run with 1000 m of padding. Subsurface storage errors represent the difference in total subsurface storage for a volume extending 100 m around the orchard and to the bottom of the model domain.

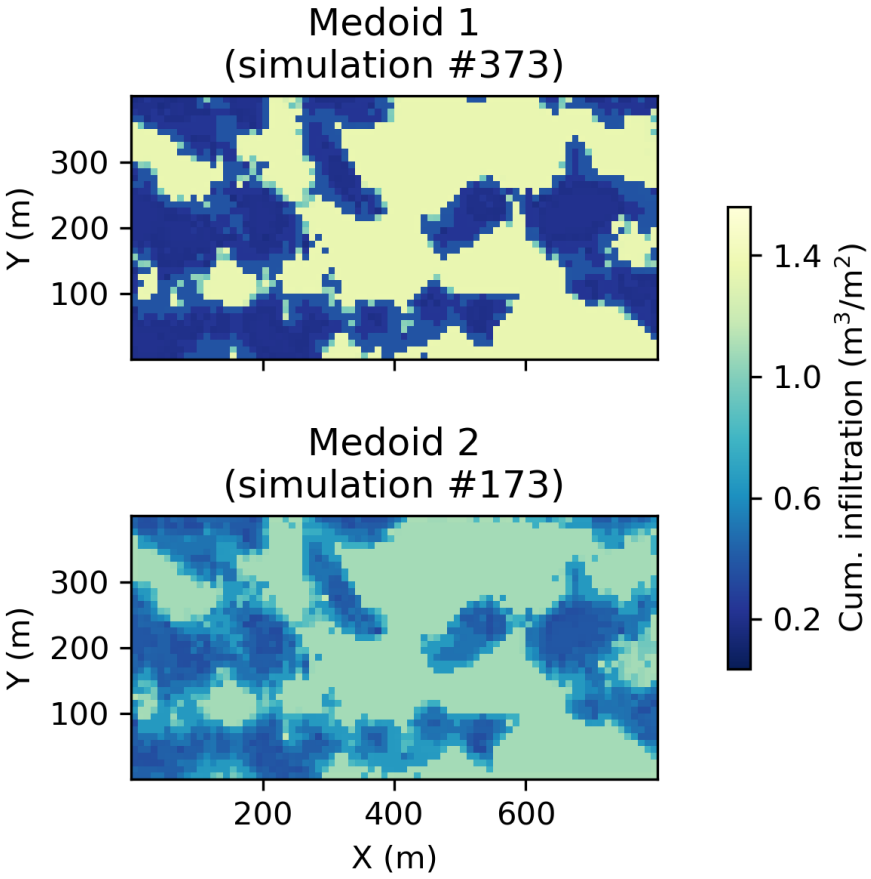

Figure S6. Cumulative infiltration maps for the medoids of the two clusters identified through *k*-medoid clustering. Maps only include surface cells within the bounds of the almond orchard because adjacent surface cells were not inundated.

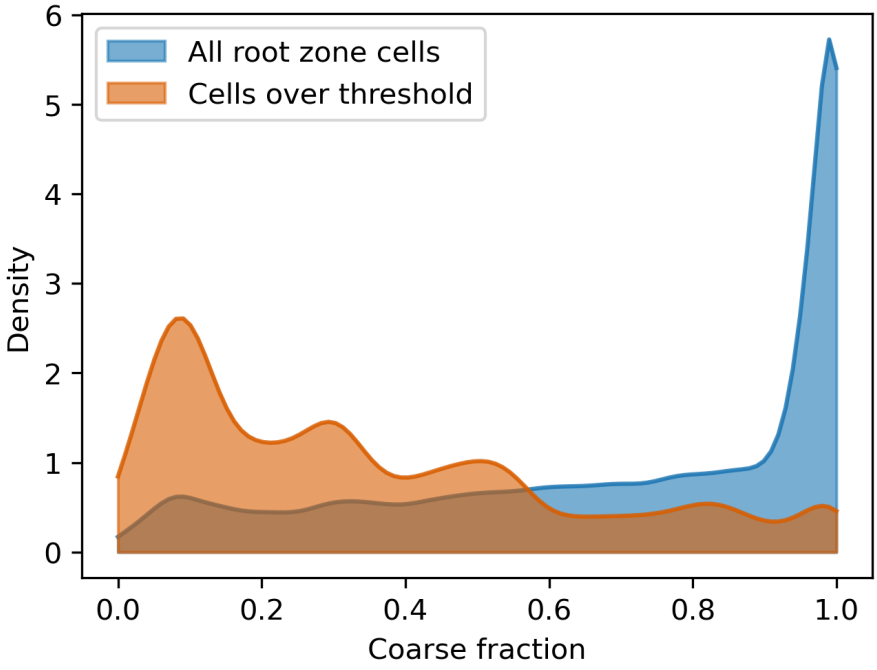

Figure S7. Conditional probability density functions of the coarse fraction of cells saturated longer than 48 hours (green) and less than 48 hours (blue). Probability density functions were generated from empirical distributions using Gaussian kernel density estimation.

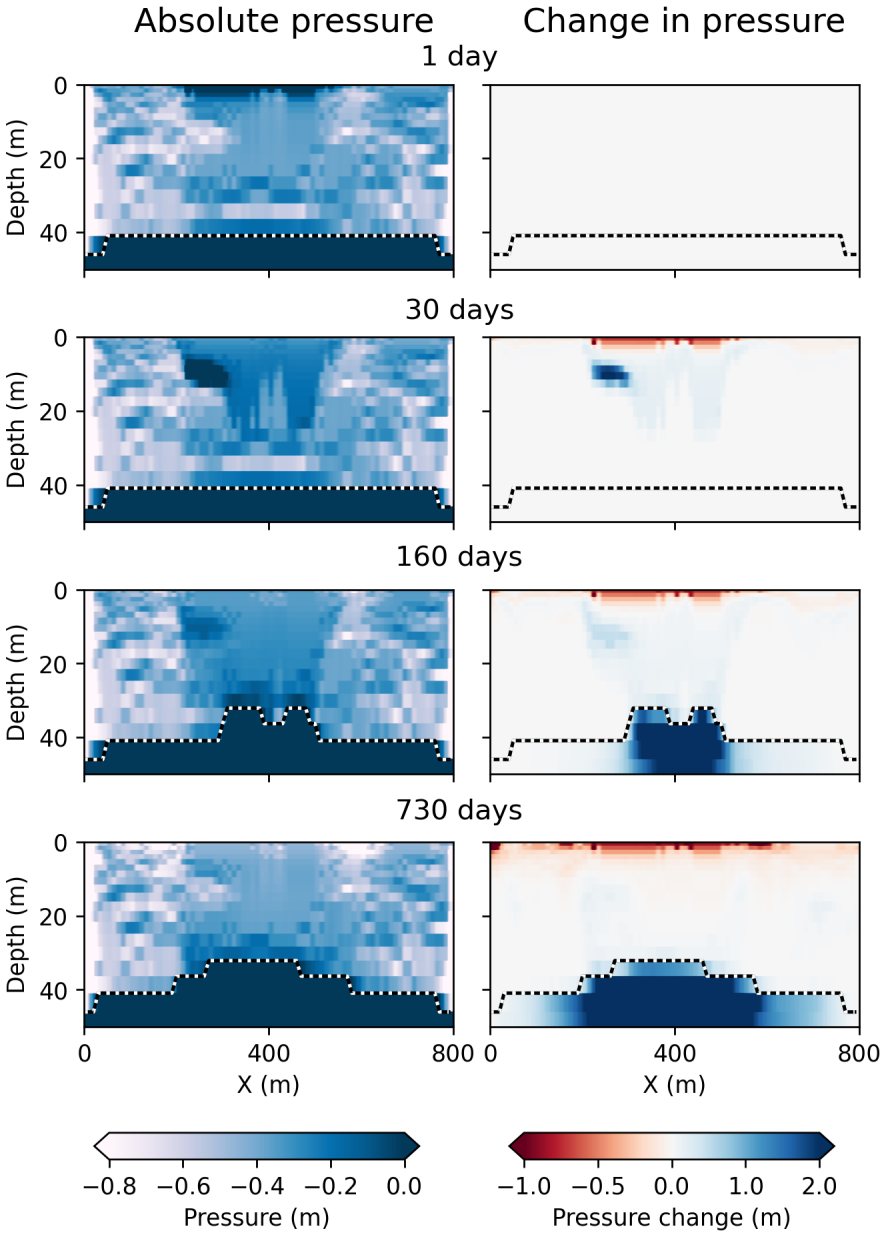

Figure S8. Vertical cross-section of absolute pressure (left) and change in pressure since inundation (right) for a single simulation for 2 years (730 days) following inundation. Each panel corresponds to the same simulation as is plotted in Fig. 6 in the main text. The dashed line shows the position of the water table, with obvious water table mounding at 160 and 730 days. Only the upper 50 m of the model domain is shown.

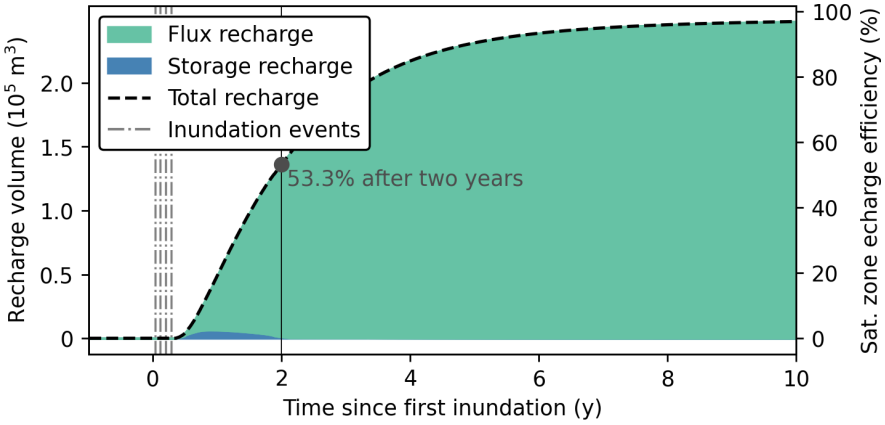

Figure S9. Temporal changes in the two components of recharge efficiency — storage recharge (blue) and flux recharge (green) — for a single simulation for 10 years following inundation. Flux recharge is cumulative over time, while storage recharge is transient. The recharge efficiency of this simulation is 53.3% after two years (vertical solid line) and, though recharge volume continues to increase beyond two years, it plateaus near 95%.